Journal of Hepatocellular Carcinoma

Dovepress
Taylor & Francis Group

Open Access Full Text Article

ORIGINAL RESEARCH

A Refined Prognostic Model for Postoperative Overall Survival in Hepatocellular Carcinoma Based on CODEX-Based Multiproteomics and Radiomics

Yuxian Wu[1,*], Jianmin Wu[2,3,*], Shaofeng Duan[4,*], Dong Liu[1,*], Wanmin Liu[5], Kairong Song[1], Juan Zhang[1], Yayuan Feng[1], Sisi Zhang[1], Yiping Liu[1], Hui Dong[6], Hao Zhang[7], Lei Chen[2,8], Ningyang Jia[1]

[1]Department of Radiology, Eastern Hepatobiliary Surgery Hospital, Third Affiliated Hospital of Naval Medical University, Shanghai, People's Republic of China; [2]The International Cooperation Laboratory on Signal Transduction, Eastern Hepatobiliary Surgery Hospital, Naval Medical University, Shanghai, People's Republic of China; [3]Shanghai Key Laboratory of Metabolic Remodeling and Health, Institute of Metabolism and Integrative Biology, Fudan University, Shanghai, People's Republic of China; [4]Precision Health Institution, GE Healthcare, Shanghai, People's Republic of China; [5]Department of Radiology, Tongji Hospital, Shanghai, People's Republic of China; [6]Department of Pathology, Eastern Hepatobiliary Surgery Hospital, Third Affiliated Hospital of Naval Medical University, Shanghai, People's Republic of China; [7]Department of Neurosurgery, Naval Medical Center of PLA, Second Military Medical University, Shanghai, People's Republic of China; [8]National Center for Liver Cancer, Shanghai, People's Republic of China

*These authors contributed equally to this work

Correspondence: Ningyang Jia, Department of Radiology, Department of Radiology, Eastern Hepatobiliary Surgery Hospital, Third Affiliated Hospital of Naval Medical University, Shanghai, People's Republic of China, Email ningyangjia@163.com; Lei Chen, The International Cooperation Laboratory on Signal Transduction, Eastern Hepatobiliary Surgery Hospital, Naval Medical University, Shanghai, People's Republic of China, Email chenlei@smmu.edu.cn

Purpose: This study aimed to develop a predictive model for the prognosis of patients with hepatocellular carcinoma (HCC) after resection.

Methods: Eighty-two HCC patients were randomly divided into a training cohort (n = 62) and a validation cohort (n = 20). Clinicopathological, multiproteomics features based on CO-Detection by Indexing (Codex), and radiomics features extracted from magnetic resonance imaging (MRI) were used to construct four models: clinicopathological model, radiomics model, proteomics model, and combined model. Model performance was evaluated using the C-index, calibration curves, receiver operating characteristic (ROC) curves, survival curves, and decision curve analysis (DCA).

Results: The combined model, integrating clinicopathological, radiomics, and multi-proteomic features, demonstrated the best performance of overall survival (OS) prediction in both the training cohort (C-index = 0.821, 95% CI: 0.745–0.897) and validation cohort (C-index = 0.791, 95% CI: 0.628–0.954). The calibration curve showed high accuracy of the combined nomogram in predicting OS.

Conclusion: This study innovatively integrates CODEX-based multiproteomics, radiomics, and clinicopathological features to construct a prognostic prediction model for HCC. The combined model demonstrates improved prognostic predictive efficacy compared with single-modality models. This approach establishes a theoretical foundation for personalized diagnosis and treatment. However, its clinical utility requires further validation through large-scale, multi-center studies.

Keywords: hepatocellular carcinoma, radiomics, codex, magnetic resonance imaging, overall survival

Introduction

Primary liver cancer was the fifth most prevalent cancer globally and the third leading cause of cancer-related deaths worldwide in 2020.[1] Notably, hepatocellular carcinoma (HCC) is the most common subtype of primary liver cancer, accounting for over 90% of cases.[2] Although the incidence and mortality rates of liver cancer have decreased in China since the late 1970s,[3,4] it remains a significant social burden. Surgical resection is recommended as a curative treatment option for HCC,[2] with resection and ablation achieving excellent survival outcomes for early stages of HCC,[5,6] resulting in a 5-year survival rate ranging from 60% to 70%. However, many patients have a poor long-term prognosis due to the advanced stage at diagnosis and the high incidence of postoperative recurrence. A 5-year recurrence rate ranging from

Received: 9 March 2025
Accepted: 19 September 2025
Published: 26 September 2025

60% to 100% is also a significant risk factor for poor prognosis.[7–11] Therefore, it is essential to identify effective methods for predicting the prognosis of HCC, enabling personalized management and treatment decisions for patients with HCC, ultimately improving their prognosis.

Medical imaging has played an important role in HCC screening, diagnosis, tumor staging, and surveillance,[12] and several prognostic factors affecting survival have been identified, such as vascular invasion and portal vein tumor thrombus.[13] However, inter-reader variability remains a limitation, and the prognosis of HCC is influenced by multiple factors. Therefore, more reliable methods are needed to predict outcomes in HCC patients and to provide a basis for adjusting postoperative treatment strategies.

Over the last decade, radiomics has emerged as a non-invasive and powerful computer-aided technique. It has improved diagnostic accuracy and prognostic prediction by extracting high-throughput imaging features from medical images that are not observed by the naked eye and converting them into quantitative data.[14,15] The main applications of radiomics in HCC involve predicting microvascular invasion (MVI), overall survival (OS), recurrence-free survival (RFS), histology, treatment response, and genetic signatures.[16–21] A meta-analysis[22] of twenty-seven studies showed that radiomics had good predictive value for MVI in HCC. A recent study by Feng et al reported that a radiopathomics nomogram outperformed either the radiomics or pathomic signatures alone in predicting OS in HCC, with an increased C-index from 0.739 to 0.840 in the training cohort and from 0.724 to 0.875 in the validation cohort.[23] Similarly, another investigation[24] demonstrated that a combined model integrating clinical data and radiomics achieved higher predictive efficacy than either the clinical score or the radiomics model alone, highlighting the complementary value of multi-source information. These findings collectively suggest the superior predictive performance of multifactorial approaches for prognostic prediction in HCC.

In addition, it has been reported that the tumor microenvironment (TME) is associated with tumor formation, survival, and metastasis.[25] In HCC, FOXP3 suppresses tumor progression via the TGF-β/Smad2/3 signaling pathway,[26] whereas hypoxia-inducible factor 1α (HIF-1α) drives infiltration of tumor-associated neutrophils (TANs), accelerating HCC progression.[27] M2-type tumor-associated macrophages (TAMs) are activated by Th2-type cytokines or other anti-inflammatory factors, such as IL-4 and IL-10, promoting tumor progression by secreting angiogenic factors and tumor growth-promoting molecules.[28] Although existing studies have confirmed the important role of biomarkers in HCC prognosis, most have been limited to analyzing correlations with only a few markers.

We speculate that integrating a broader panel of biomarkers may enable more accurate prediction of HCC prognosis. Considering that current applications of biomarkers in the prognostic assessment of HCC mostly involve the analysis of only a limited number of indicators, and that no existing study has systematically integrated the associations between numerous proteomic features and HCC prognosis, this study proposes constructing a combined predictive model integrating radiomics, multi-proteomic features based on CO-Detection by Indexing (CODEX) and clinicopathological characteristics. CODEX is a commercially available multiplexed tissue imaging tool (Akoya Biosciences, Menlo Park, California, USA). It uses DNA-conjugated antibodies, iterative polymerase extension with fluorescent nucleotides, and chemical fluorophore cleavage to achieve high-parameter immunofluorescence imaging of fresh-frozen tissue, formalin-fixed paraffin-embedded (FFPE) tissue, and tissue microarrays (TMAs).[29,30] Compared with traditional immunohistochemistry (which can detect a maximum of 7 markers), this technology allows simultaneous detection of up to 60 protein markers in a single tissue section with single-cell resolution.[30,31] Quantitative analysis of image data using supporting software enables precise measurement of marker expression levels and cell counts, providing data support for TME research and facilitating the discovery of biomarkers and therapeutic targets.[30,32]

By integrating multidimensional information, this model is expected to overcome the limitations of traditional single-modal or limited-indicator analyses and provide a new quantitative tool for precise prediction of prognosis in HCC patients.

Methods

Patients

An overview of this study design is shown in Figure 1. The study was conducted in accordance with the 1964 Helsinki Declaration and its later amendments or comparable ethical standards, and was approved by the Medical Ethics Committee of the Third Affiliated Hospital of Naval Medical University (No. EHBHKY2002-H-P002), which determined that the

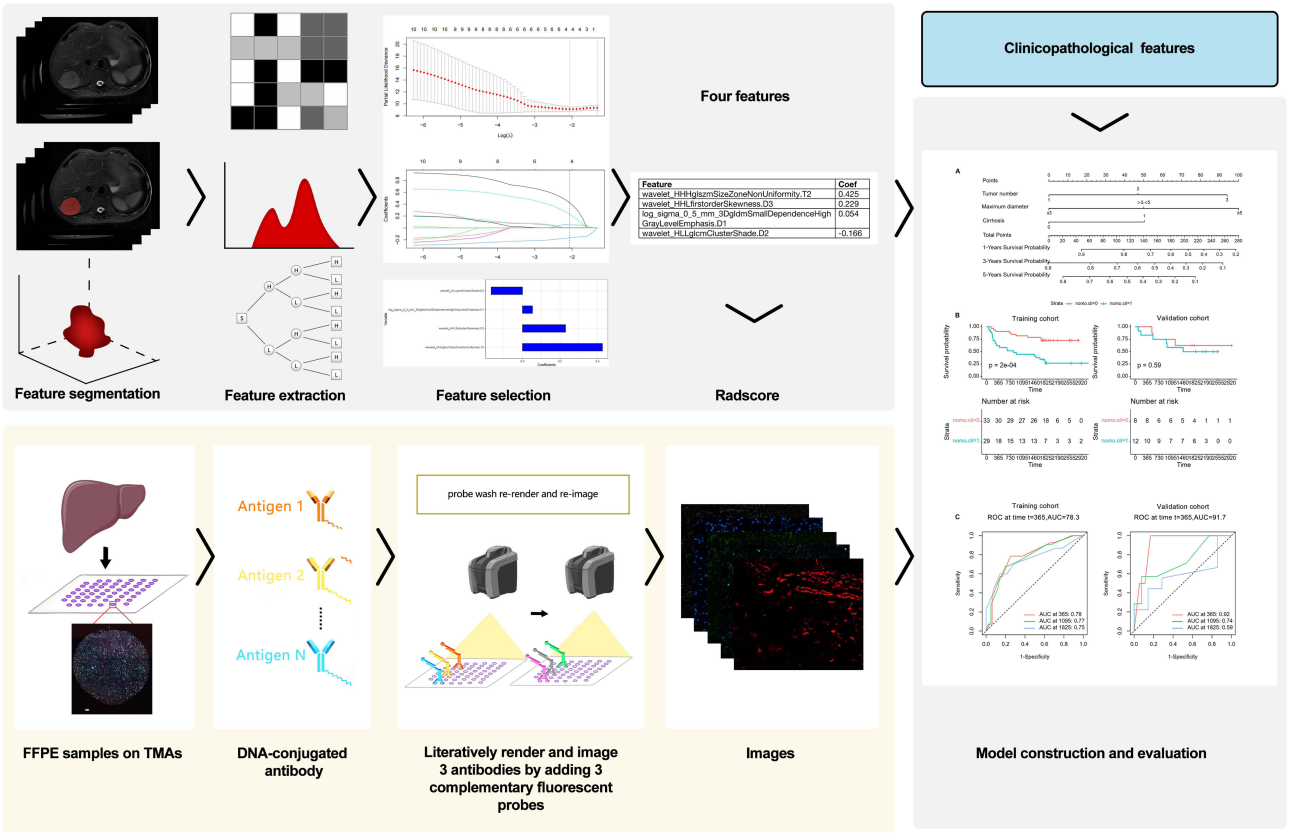

Figure 1 The workflow of this study.

anonymized data processing met ethical requirements, thus exempting the need for informed consent procedures. A total of 424 patients who underwent CODEX analysis after surgery and received a pathological diagnosis of HCC at our hospital between January 2010 and December 2016 were initially enrolled. The inclusion criteria were as follows: (1) No preoperative anti-tumor therapies; (2) No history of other tumors; (3) No distant metastasis; (4) underwent enhanced magnetic resonance imaging (MRI) within 4 weeks before surgery; and (5) complete postoperative follow-up data. The exclusion criteria were: (1) Pathological diagnosis of combined HCC-cholangiocarcinoma or cholangiocarcinoma; (2) Incomplete clinical pathological or follow-up data; (3) Incomplete preoperative enhanced MRI data. Finally, a total of 82 patients (73 men and 9 women, aged 55.78 ± 11.93 years) were included in the study. All enrolled patients were randomly divided into a training cohort (n = 62) and a validation cohort (n = 20) in a ratio of 7.5: 2.5. The process of patient selection is shown in Figure 2.

Follow-Up

All patients had complete postoperative follow-up data. Patients were consistently followed up at intervals of 3 to 6 months for the first 2 years after surgery and once a year for the next 3 years. The termination point for follow-up was 60 months after the operation. Postoperative routine examinations included routine blood tests, serum biochemistry, serum alpha-fetoprotein (AFP) levels, and contrast-enhanced CT/MRI. OS was the primary endpoint of this study, defined as the time from the date of surgery to the date of death or last follow-up.

Clinical and Pathological Features

Preoperative clinical characteristics and postoperative pathological features were collected from medical records, including sex, age, viral infection status of hepatitis B (HBV), alpha-fetoprotein (AFP), Child-Pugh score, Barcelona Clinic Liver Cancer (BCLC) stages, tumor number, tumor maximum diameter, liver cirrhosis, portal-vein tumor

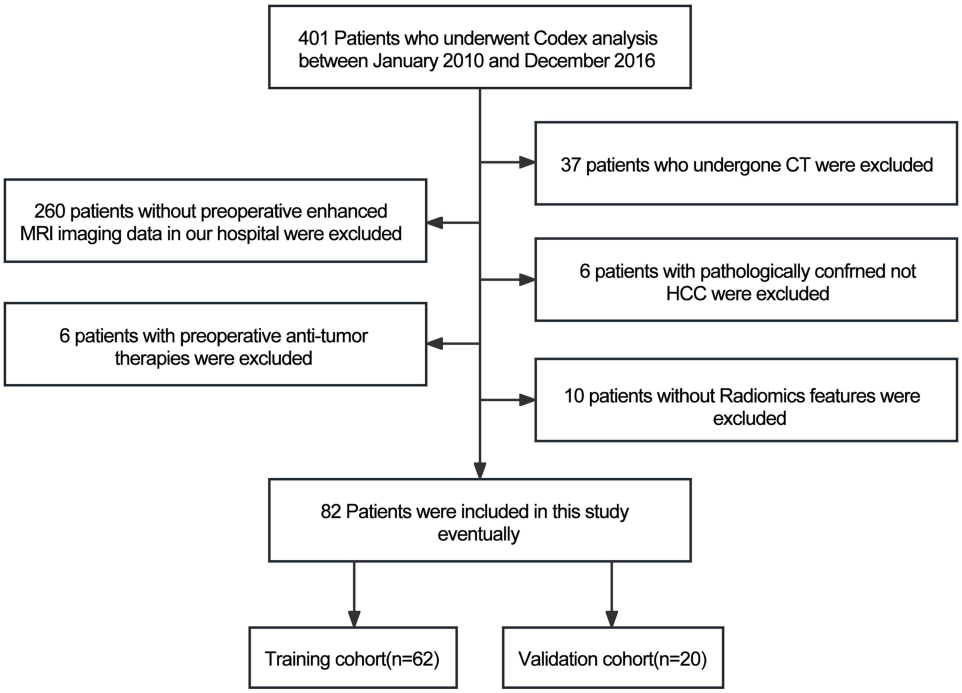

Figure 2 Flowchart illustrating the patient selection process. HCC, hepatocellular carcinoma.

thrombus, MVI status, and capsule (Table 1). All pathological features were assessed by two experienced pathologists in liver pathology.

Protein Data and Image Acquisition by CODEX

In this study, 34 biomarkers were selected from CODEX staining: FoxP3, p-mTOR, Twist1, PD-L1, p53, p-AMPK, PD-1, c-Myc, Caspase-3, CD163, CD45, HIF-1α, CD45RO, CD107A, α-SMA, CD21, CD68, Hepar1α/HepPar 1, CD8, CD3,

Table 1 Demographic and Clinicopathological Characteristics of Patients in the Training Cohort and Validation Cohort

Characteristics	Training Cohort	Validation Cohort	*p* Value
Sex			0.802
Male	56(90.3%)	6(9.7%)	
Female	17(85%)	3(15%)	
Age	55.74±12.117	55.9±11.634	0.697
Hepatitis B virus antigen			0.458
Yes	41(66.1%)	15(75%)	
No	21(33.9%)	5(25%)	
AFP (ng/mL)			0.295
<20	33(53.2%)	11(55.0%)	
≤400	14(22.6%)	7(35.0%)	
>400	15(24.2%)	2(10.0%)	

(*Continued*)

Table 1 (Continued).

Characteristics	Training Cohort	Validation Cohort	*p* Value
BCLC stage			0.705
0	2(3.2%)	0(0%)	
A	37(59.7%)	13(65.0%)	
B	15(24.2%)	3(15.0%)	
C	8(12.9%)	4(20.0%)	
Child-pugh score			0.531
Class A	60(96.8%)	18(90%)	
Class B	2(3.2%)	2(10%)	
Maximum diameter (cm)			0.533
≤3	6(9.7%)	1(5.0%)	
>3, <5	20(32.3%)	9(45%)	
≥5	36(58.1%)	10(50%)	
Tumor number			1.000
1	44(71%)	14(70%)	
2	9(14.5%)	3(15%)	
3	9(14.5%)	3(15%)	
Portal-vein tumor thrombus			0.802
Yes	6(9.7%)	3(15%)	
NO	56(90.3%)	17(85%)	
MVI			0.81
Yes	26(41.9%)	9(45.0%)	
No	36(58.1%)	11(55.0%)	
Cirrhosis			0.012
Yes	18(29%)	12(60%)	
No	44(71%)	8(40%)	
Capsule			0.476
Yes	11(17.7%)	5(25%)	
No	51(82.3%)	15(75%)	

Notes: *p* value<0.01 indicates a significant difference between the training and validation cohorts.
Abbreviations: AFP, alpha-fetoprotein; BCLC, the Barcelona Clinic Liver Cancer staging system; MVI, microvascular infiltration.

Glypican3, Keratin, CD4, p-S6, Ki-67, Vimentin, E-cadherin, HLA-DR, CD44, HistoneH3, CD20, Podoplanin, CD31, and Pan-CK.

Formalin-fixed paraffin-embedded (FFPE) tissue and tissue microarrays (TMAs) were used in our study. Tissue samples were obtained from postoperative HCC patients at Eastern Hepatobiliary Surgery Hospital. Written informed consent was

obtained from all patients. CODEX processor software (Akoya Biosciences, version 1.7) was used to process the CODEX images. CODEX Multiplex Analysis Viewer (Akoya Biosciences, version 1.5.0.8) was used to analyze the protein expression in each sample. All biomarker data were normalized using the CODEX Multiplex Analysis Viewer. The detailed procedures can be found in the supplementary files. The CODEX workflow is shown in Figure 1. Images of a single tissue region colored for each antibody are shown in Figure 3A.

MRI Image Acquisition, Tumor Segmentation, and Radiomics Feature Extraction

The complete radiomics workflow is shown in Figure 1. All patients underwent abdomen-enhanced MRI within 4 weeks before surgery, including axial T2-weighted imaging with fat suppression (T2WI-FS), T1-weighted imaging (T1WI), and postcontrast dynamic-enhanced T1WI in the arterial phase (AP), portal venous phase (PVP), and delayed phase (DP) scans performed using a 1.0/1.5-T scanner.

The tumour regions of interest (ROIs) in the MR images were manually delineated using ITK-SNAP 4.0.0 software (http://www.itksnap.org). A radiologist with 5 years of experience manually segmented ROIs from MRI images (five phases), and a radiologist with 7 years of experience confirmed the results. In case of disagreement, consensus was reached through discussion. Two weeks later, one radiologist (Reviewer 1) randomly selected 20 HCC patients and re-segmented the ROIs to assess the intraclass correlation coefficient (ICC) within the group. Additionally, another radiologist (Reviewer 2) independently drew the ROIs for another randomly selected set of 20 HCC patients to evaluate the inter-rater reliability. ICC values greater than 0.75 represented good agreement between the reviewers.

Radiomics features were extracted from ROIs using 3D Slicer (version 4.9.0, http://www.slicer.org). Eventually, a total of 1223 features were extracted from T1WI, T2WI, arterial, portal venous, and delayed sequences, giving a total of 6115 features for each lesion and covering shape, first-order statistical features, texture features, and wavelet decomposition.

Rad-Score Construction

To select the radiomics features, we followed three key steps. First, we utilized univariate Cox regression analysis on the training cohort and retained radiomics features with a p value < 0.05 for further analysis. Subsequently, we conducted Pearson's correlation analysis to investigate the correlation among individual features. For pairs of features with a correlation coefficient > 0.9, one feature was eliminated. Finally, we employed the least absolute shrinkage and selection operator (LASSO) Cox regression method with five-fold cross-validation to select the optimal radiomics features from the training cohort for building the radiomics score (Rad-score). The Rad-score for each patient was calculated via a linear combination of the features weighted according to their corresponding coefficients in the LASSO Cox regression method.

Model Construction and Validation

We established three models for OS prediction: The clinicopathological model included clinical data available before surgery and post-operative pathological variables; The proteomics model included CODEX-based multi-protein features. The combined model included the aforementioned predictors plus and Radscore. Predictors of OS with statistical significance in the univariate Cox regression analysis were included in the multivariate Cox regression; the final model was selected by backward stepwise elimination with Akaike Information Criterion(AIC). The three models incorporating their respective independent predictors, were developed and presented as three separate nomograms.

The performance of the Rad-score, clinicopathological model, proteomics model and combined model was evaluated using the concordance index (C-index) and the area under the curve (AUC) of the time-dependent receiver operating characteristic (ROC) curve in the training cohort and confirmed in the validation cohort. Survival curves were created using the Kaplan-Meier (KM) method and compared using a two-sided Log rank test in all models. Patients were stratified into low- or high-risk groups based on the median value of each model score. Calibration curves were plotted to analyze the prognostic performance of the four nomograms in both the training and validation cohorts. Decision curve analysis (DCA) was performed to evaluate the benefit of the prediction models for clinical decision-making.

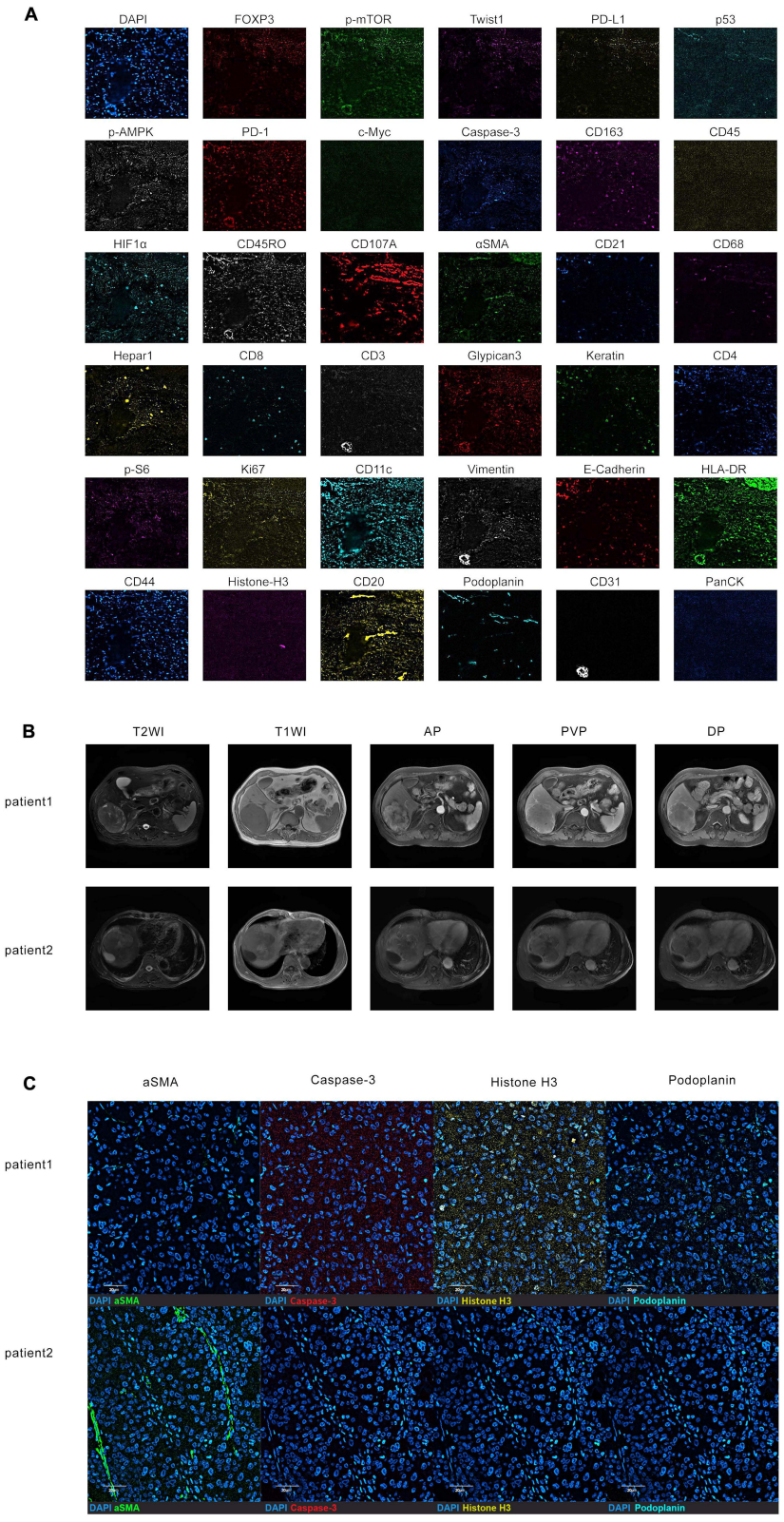

Figure 3 Images of a single tissue region colored for each antibody. Scale bar, 10 μm **(A)**. Representative HCC patients with their MRI images and CODEX images **(B** and **C)**. MRI images of T2WI-FS, T1WI, AP, PVP, and DP for these patients (**B**). CODEX images of four proteins (α-SMA, Caspase-3, Histone H3, and Podoplanin) in these patients (**C**). Patient 1: male, tumor maximum diameter of 8.0 cm, died at 25 months, exhibited high levels of Caspase-3 and Histone H3, and low levels of α-SMA and Podoplanin. Patient 2: male, tumor maximum diameter of 7.6 cm, alive at 60 months, exhibited low levels of Caspase-3 and Histone H3, and high levels of a-SMA and Podoplanin.

https://doi.org/10.2147/JHC.S527066

Statistical Analysis

All statistical analyses were performed using R software (version 3.5.2; R Foundation for Statistical Computing, Vienna, Austria) and SPSS software (version 26.0; IBM, New York, NY). A two-side p value < 0.01 was considered statistically significant. Continuous variables were compared using the t-test or Wilcoxon test, while categorical variables were compared using the chi-square or Fisher's exact test, as appropriate. Univariate and multivariate Cox regression analyses were performed using the Cox proportional hazards model to identify predictors of OS. Features with a p value < 0.1 in the univariate Cox regression were included in the multivariate Cox regression. Stepwise backward elimination was employed to iteratively remove non-significant predictors, sequentially refining the model until the optimal combination of variables was identified, as determined by the minimized Akaike Information Criterion (AIC). The performance of the four models was evaluated using Harrell's C-index and the AUC of the time-dependent ROC. Survival curves were generated using the KM method and compared using Log rank tests. Patients in all four models were divided into high- and low-risk groups according to the optimal cutoff values for each model. Calibration curves were used to evaluate the alignment of nomograms (ie, how closely the predicted probabilities corresponded with the observed outcomes). The correlation of DCA curve analysis was assessed using Spearman's rank correlation coefficient.

Results

Patients' Characteristics

Among the 424 patients who underwent CODEX analysis, 324 were excluded as shown in Figure 2. A total of 82 patients met the inclusion criteria and were included in the study. Patient demographics and clinicopathological features are presented in Table 1. Among them, 73 (89.0%) were male, and the median age of all patients was 58 years (range, 26–89 years). The median OS was 57.1 months (range, 2.1–111.8 months) in the training cohort and 58.8 months (range, 2.9–97.7 months) in the validation cohort. There were no statistically significant differences in clinical or pathological characteristics between the two groups (Table 1).

Rad-Score Construction

Finally, four radiomics features were selected using LASSO Cox regression for predicting OS and used to build the radiomics score. The radiomics score was calculated by combining the selected features and their corresponding weights using the following formula:

Rad-score = 0.425 × wavelet_HHH_glszm_SizeZoneNonUniformity_T2WI + 0.229 × wavelet_HHL_firstorder_Skewness_DP + 0.054 × log_sigma_0_5_mm_3D_gldm_SmallDependenceHighGrayLevelEmphasis_AP − 0.166 × wavelet_HLL_glcm_ClusterShade_PVP.

The radiomics score demonstrated good predictive performance for OS in HCC, with a C-index of 0.736 (95% CI: 0.648, 0.824) in the training cohort and 0.709 (95% CI: 0.560–0.858) in the validation cohort (Table 2).

Table 2 Performance of Each Model for Predicting OS in HCC Patients

Model	Training Cohort (n=62)			Validation Cohort (n=20)		
	C-index[95% CI]	SE	*p* value	C-index[95% CI]	SE	*p* value
Rad	0.736[0.648, 0.824]	0.045	0.154*	0.709[0.560, 0.858]	0.076	0.466*
Cli	0.713[0.621, 0.805]	0.047	0.071**	0.675[0.481, 0.869]	0.099	0.369**
Pro	0.696[0.594, 0.798]	0.052	0.053***	0.731[0.588, 0.874]	0.073	0.587***
Cli+Pro+Rad	0.821[0.745, 0.897]	0.039		0.791[0.628, 0.954]	0.083	

Note: *Rad vs Cli+Pro+Rad *p* value. **Cli vs Cli+Pro+Rad *p* value. ***pro vs Cli+Pro+Rad *p* value.
Abbreviations: CI, confidence interval.

COEDX Images and Selected Biomarkers

Codex images of 34 biomarkers in a single tissue region are shown in Figure 3A, with different colors representing the expression of the corresponding proteins. All biomarkers were normalized and quantitatively analyzed using the CODEX Multiplex Analysis Viewer. The CODEX and MRI images of representative HCC patients with high and low survival rates are shown in Figure 3B and C. These patients had similar tumor maximum diameters and MRI features. The CODEX images showed that the patient with high levels of Caspase-3 and Histone H3, and low levels of α-SMA and Podoplanin had a worse prognosis and died 25 months after surgery. In contrast, the patient with low levels of Caspase-3 and Histone H3 and high levels of α-SMA and Podoplanin had a better prognosis and survived for 60 months.

Development and Validation of OS Prediction Models

In the training cohort, variables were predictive of HCC OS at univariable analysis. With use of stepwise multivariable analysis with the lowest AIC score, independent predictors were identified for the clinicopathological model, proteomics model and combined models (Supplementary Tables 1, 2 and Table 3). Three models above that integrated corresponding independent predictors were developed and presented as three nomograms (Supplementary Figures 1A, 2A and Figure 4A). The clinicopathological model was built based on tumor number, maximum diameter, and cirrhosis (Supplementary Table 1). The proteomics model was built based on Caspase-3, a-SMA, Histone H3, and Podoplanin (Supplementary Table 2). The radiomics model was based on the rad-score. The combined model was built based on rad-score, tumor number, maximum diameter, cirrhosis, Caspase-3, and Histone H3 (Table 3). The contributions of the four radiomics features to the final model are shown in Supplementary Table 3.

The performance of each model was evaluated by calculating the C-index values (Table 2). Notably, the combined model demonstrated the highest performance in the training cohort, with a C-index of 0.821 (95% CI, 0.745–0.897). This was followed by the radiomics model, which had a C-index of 0.736 (95% CI, 0.648–0.824), and the clinicopathological model, which had a C-index of 0.713 (95% CI, 0.621–0.805). The proteomics model had the lowest predictive performance in the training cohort, with a C-index of 0.696 (95% CI, 0.594–0.798). In the validation cohort, the combined model continued to show the best performance, with a C-index of 0.791 (95% CI, 0.628–0.954). This was followed by the proteomics model, which had a C-index of 0.731 (95% CI, 0.558–0.874). The clinicopathological model had the lowest predictive performance in this group, with a C-index of 0.675 (95% CI, 0.481–0.869). Overall, the combined model demonstrated superior performance in both the training and validation cohorts.

The KM curves and Log rank tests for estimating OS are shown in Figure 4B and Supplementary Figures 1B, 2B and 3B. In the training cohort, patients in the low-risk group exhibited significantly better outcomes compared to those in the high-risk

Table 3 Univariate and Multivariate Cox Regression Analyses of Independent Predictors for the Combined Model

Risk Factor	Univariate Analysis		Multivariate Analysis	
	HR [95% CI]	*p value*	HR [95% CI]	*p value*
Radscore	6.03 [3.17; 11.47]	< 0.001	7.98 [3.60; 17.65]	< 0.001
Tumor number	1.94 [1.26; 2.98]	0.002	1.85 [1.18; 2.90]	0.007
Maximum diameter	1.78 [0.96; 3.31]	0.069	2.05 [0.90; 4.64]	0.086
Cirrhosis	1.93 [0.93; 4.02]	0.077	2.23 [0.94; 5.27]	0.067
Caspase-3	16.58 [1.71; 160.41]	0.015	17.27 [0.95; 313.75]	0.054
αSMA	2.59×10^{-6} [1.80×10^{-11}; 0.37]	0.033		
HistoneH3	14.28 [1.11; 182.98]	0.041	13.33 [0.85; 208.04]	0.065
Podoplanin	3.54 [0.83; 15.03]	0.087		

Abbreviations: HR, Hazard Ratio; CI, confidence interval.

https://doi.org/10.2147/JHC.S527066

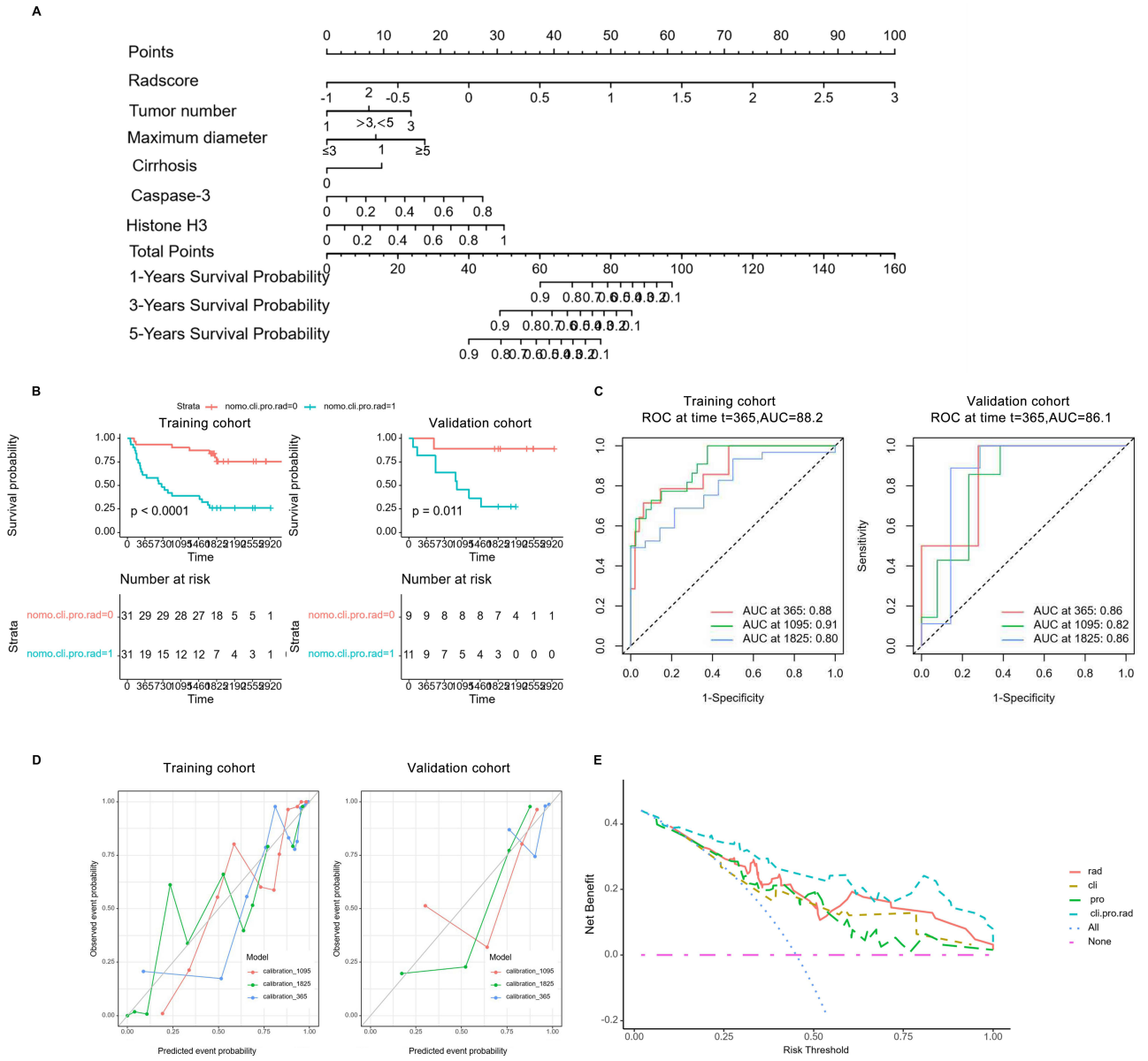

Figure 4 Development and evaluation of the combined nomogram for predicting OS in HCC patients **(A–E)**. The nomogram was constructed based on the corresponding independent predictors(**A**). KM curves of the combined model in the training cohort and the validation cohort (**B**). ROC curves of the combined model for predicting OS in HCC patients at 1, 3, and 5 years after surgery in the training cohort and the validation cohort (**C**). Calibration curves of the combined model in both the training cohort and validation cohort **(D)**. DCA of all models **(E)**. The *x*-axis indicates the risk threshold probability, and the *y*-axis measures the net benefit. The combined model (cli.pro.rad line) for HCC OS prediction demonstrates the highest benefit among all models. The combined model showed a higher net benefit than the other three models across most ranges of reasonable threshold probabilities.

Abbreviations: OS, overall survival; KM, Kaplan–Meier.

group (log-rank $p < 0.05$) when assessed using the four models. Similar results were found in the validation cohort ($p < 0.05$) for only the combined and proteomics models. The OS significantly differed between HCC patients stratified by the proteomics and combined models ($p < 0.05$ in both the training and validation cohorts).

The ROC curves were plotted to assess the predictive performance of all models for 1-year, 3-year, and 5-year OS (Figure 4C and Supplementary Figures 1C, 2C, 3C). The combined model showed excellent performance in predicting OS at these time points, with AUCs of 0.88, 0.91, and 0.80, respectively, in the training cohort, and 0.86, 0.82, and 0.86, respectively, in the validation cohort. It outperformed the radiomics model (AUCs of 0.80, 0.83, and 0.70, respectively, in the training cohort, and 0.78, 0.67, and 0.81, respectively, in the validation cohort), the clinicopathological model (AUCs of 0.78, 0.77, and 0.75, respectively, in the training cohort, and 0.92, 0.74, and 0.59, respectively, in the validation

cohort), and the proteomics model (AUCs of 0.69, 0.75, and 0.57, respectively, in the training cohort, and 0.78, 0.68, and 0.78, respectively, in the validation cohort). The calibration curves demonstrated good agreement between the actual observed outcomes and the predicted survival rates from the combined nomogram in both the training and validation cohorts (Figure 4D).

Furthermore, we constructed DCA curves to assess the predictive accuracy of various models and their relevance in clinical decision-making. The DCA curve analysis revealed that the combined model offered higher net benefits compared to the other models (Figure 4E).

Discussion

Previous studies have identified several factors that impact prognosis, including age, tumor number, tumor size, clinical staging, pathological grading, microvascular invasion (MVI), and various biomarkers.[33–37] Given the heterogeneity of HCC and its variable outcomes, an effective prediction model that incorporates multiple influencing factors is essential. Our combined model exhibited improved performance in predicting OS of HCC patient. The combined model revealed that tumor number, maximum diameter, cirrhosis, rad-score, Caspase-3, and Histone H3 are the independent predictors of OS in HCC patients.

Radiomics differs from conventional imaging techniques in that it uses artificial intelligence (AI) methods to extract key image features and obtain accurate quantitative data from medical images for analysis.[38] Deng[39] et al demonstrated a radiomics signature for predicting OS in HCC with a C-index of 0.689 (95% CI, 0.626–0.751). In our study, the radiomics model exhibited good OS prediction performance, with a C-index of 0.736 (95% CI, 0.648–0.824). Patients with higher rad-scores were found to have significantly lower OS compared to those with lower rad-scores. When combined with clinicopathological-imaging risk factors and multiproteomics, the combined model significantly improved OS prediction in HCC patients, achieving a C-index of 0.821 (95% CI, 0.745–0.897). Although there were no statistically significant differences, this suggests that the combined model offers more reliable OS prediction value for HCC patients.

CODEX, as a novel tool capable of quantitatively detecting multiple proteins, has been proven to be practical.[29–31] In our study, we innovatively introduced this technology and constructed a model by combining it with radiomics and clinical indicators, which improved the predictive performance of the HCC prognostic model. The results showed that Histone H3 and caspase-3 were identified as independent predictors of OS in the combined model. Patients with low expression of caspase-3 and Histone H3 had a more favorable OS, suggesting that higher expression correlates with a poor prognosis. Niu et al demonstrated that phosphorylation of histone H3 at residue Thr11 can lead to the transcription of Dickkopf-1 (DKK1) in HCC.[40] Furthermore, overexpression of DKK1 was found at the transcript level in HCC, promoting cell migration and invasion.[41,42] Jing et al discovered that overexpression of histone H3 is present in clinical HCC patients and that histone H3 promotes the proliferation and metastasis of HCC cells both in vitro and in vivo.[43]

Caspase-3, a member of the cysteine protease family, has been implicated in HCC progression through the PDK1/AKT/caspase-3 signaling pathway.[44] Furthermore, caspase-3 has been shown to promote oncogenic transformation by inducing genetic instability.[45] Several studies have shown that genetic polymorphisms in caspase (CASP) genes are associated with the risk of HCC.[46–48] Zhang et al found that the haplotype TT/TG in caspase-3 was significantly associated with decreased OS and DFS in HCC patients, suggesting that polymorphisms in CASP3 may increase the risk of developing HCC and lead to poor survival outcomes by reducing apoptotic capacity.[46] The aforementioned research findings echo our study results, providing additional empirical support for our results.

Notably, the combined model's prediction performance aligns closely with actual outcomes, as indicated by the calibration curve, suggesting that it accurately estimates risk in both cohorts. Additionally, we evaluated the predictive accuracy of all models for 1-, 3-, and 5-year OS. The results indicated that the combined nomogram had superior applicability for predicting OS at multiple time points. These results highlight the value of multi-omics approaches for comprehensive HCC prognosis evaluation.

The joint prognostic model for postoperative survival of HCC developed in this study can provide guidance for the subsequent treatment of HCC. In cases where the model predicts a shorter survival period, close monitoring should be initiated. Meanwhile, various postoperative treatments, including but not limited to interventional therapy, targeted therapy, and immunotherapy, can be considered.

Our study has several limitations that deserve mention. Firstly, it is a retrospective, single-center study with a relatively small cohort of HCC patients. Insufficient sample size leads to low test power and wide confidence intervals, which in turn affect the robustness and generalizability of the model to a certain extent. We innovatively integrated CODEX technology into the construction of a prognostic model for HCC, but due to the innovation of this attempt and the lack of sufficient prior experience for reference, external validation has not yet been completed. Secondly, the proteins included in this study are limited, and incorporating additional proteins associated with HCC would be beneficial for further research. Thirdly, peritumoral-associated radiomic features and proteomics, which may also impact HCC prognosis, were not included in this study, potentially limiting the prediction accuracy. However, the combined model showed excellent prognostic performance. In future studies, we plan to expand the sample size and conduct a multicenter collaborative research project. We aim to incorporate peritumoral-associated radiomics features and proteomics data into the prediction model to improve its clinical accuracy and practicality.

Conclusions

In conclusion, this study demonstrates that a prognostic model integrating clinicalpathological, CODEX-based multi-proteomics, and radiomics features exhibits strong performance in predicting OS among patients with HCC. This model establishes a novel research direction for assessing postoperative survival. Additionally, the combined model's visual representation has potential as a tool for individualized management decisions in HCC, although its clinical utility requires further validation and systematically evaluated in large-scale, multicenter studies.

Abbreviations

HCC, Hepatocellular Carcinoma; MVI, Microvascular invasion; OS, Overall survival; RFS, Recurrence-free survival; TME, Tumor microenvironment; TAMs, Tumor-associated macrophages; HIF-1α, Hypoxia-inducible factor 1α; TAN, Tumor-associated neutrophils; FFPE, Paraffin embedded; TMAs, Tissue microarrays; CODEX, CO-detection by indexing; MRI, Magnetic Resonance Imaging; AFP, Alpha-fetoprotein; HBV, hepatitis B; BCLC, Barcelona Clinic Liver Cancer; FFPE, Formalin-fixed paraffin embedded; T2WI-FS, T2-weighted imaging with fat suppression; T1WI, T1-weighted imaging; AP, Arterial phase; PVP, Portal venous phase; DP, Delayed phase; ROI, Region of interest; ICC, Intra-class correlation coefficient; LASSO, Least absolute shrinkage and selection operator; DCA, Decision curve analysis; ROC, Receiver Operating Characteristic Curve; CT, Computed Tomography; AI, Artificial intelligence.

Data Sharing Statement

The datasets during and/or analysed during the current study available from the corresponding author on reasonable request.

Ethics Approval and Informed Consent

The study was approved by the Medical Ethics Committee of the Third Affiliated Hospital of Naval Medical University (No. EHBHKY2002-H-P002). The anonymized data processing met ethical requirements, thus exempting the need for informed consent procedures.

Author Contributions

All authors made a significant contribution to the work reported, whether that is in the conception, study design, execution, acquisition of data, analysis and interpretation, or in all these areas; took part in drafting, revising or critically reviewing the article; gave final approval of the version to be published; have agreed on the journal to which the article has been submitted; and agree to be accountable for all aspects of the work.

Funding

This study was funded by Talent Plan of Shanghai Municipal Health Commission, China (2022LJ024). The funder played no role in study design, data collection, analysis and interpretation of data, or the writing of this manuscript.

Disclosure

All authors declare no financial or non-financial competing interests in this work.

References

1. Sung H, Ferlay J, Siegel RL, et al. Global cancer statistics 2020: GLOBOCAN estimates of incidence and mortality worldwide for 36 cancers in 185 countries. *CA Cancer J Clin*. 2021;71(3):209–249. doi:10.3322/caac.21660
2. Llovet JM, Kelley RK, Villanueva A, et al. Hepatocellular carcinoma. *Nat Rev Dis Primers*. 2021;7(1):6. doi:10.1038/s41572-020-00240-3
3. Arnold M, Abnet CC, Neale RE, et al. Global Burden of 5 Major Types of Gastrointestinal Cancer. *Gastroenterology*. 2020;159(1):335–349.e15. doi:10.1053/j.gastro.2020.02.068
4. Petrick JL, Florio AA, Znaor A, et al. International trends in hepatocellular carcinoma incidence 1978-2012. *Int J Cancer*. 2020;147(2):317–330. doi:10.1002/ijc.32723
5. Livraghi T, Meloni F, Di Stasi M, et al. Sustained complete response and complications rates after radiofrequency ablation of very early hepatocellular carcinoma in cirrhosis: is resection still the treatment of choice? *Hepatology*. 2008;47(1):82–89. doi:10.1002/hep.21933
6. Roayaie S, Obeidat K, Sposito C, et al. Resection of hepatocellular cancer ≤2 cm: results from two Western centers. *Hepatology*. 2013;57(4):1426–1435. doi:10.1002/hep.25832
7. Bruix J, Gores GJ, Mazzaferro V. Hepatocellular carcinoma: clinical frontiers and perspectives. *Gut*. 2014;63(5):844–855. doi:10.1136/gutjnl-2013-306627
8. Poon RT, Fan ST, Lo CM, Liu CL, Wong J. Long-term survival and pattern of recurrence after resection of small hepatocellular carcinoma in patients with preserved liver function: implications for a strategy of salvage transplantation. *Ann Surg*. 2002;235(3):373–382. doi:10.1097/00000658-200203000-00009
9. Shah SA, Cleary SP, Wei AC, et al. Recurrence after liver resection for hepatocellular carcinoma: risk factors, treatment, and outcomes. *Surgery*. 2007;141(3):330–339. doi:10.1016/j.surg.2006.06.028
10. Villanueva A. Hepatocellular Carcinoma. *N Engl J Med*. 2019;380(15):1450–1462. doi:10.1056/NEJMra1713263
11. Lacaze L, Scotté M. Surgical treatment of intra hepatic recurrence of hepatocellular carcinoma. *World J Hepatol*. 2015;7(13):1755–60. DOI:10.4254/wjh.v7.i13.1755.
12. Miranda J, Horvat N, Fonseca GM, et al. Current status and future perspectives of radiomics in hepatocellular carcinoma. *World J Gastroentero*. 2023;29(1):43–60. doi:10.3748/wjg.v29.i1.43
13. Cabibbo G, Enea M, Attanasio M, Bruix J, Craxì A, Cammà C. A meta-analysis of survival rates of untreated patients in randomized clinical trials of hepatocellular carcinoma. *Hepatology*. 2010;51(4):1274–1283. doi:10.1002/hep.23485
14. Lambin P, Leijenaar RTH, Deist TM, et al. Radiomics: the bridge between medical imaging and personalized medicine. *Nat Rev Clin Oncol*. 2017;14(12):749–762. doi:10.1038/nrclinonc.2017.141
15. Miranda Magalhaes Santos JM, Clemente Oliveira B, Araujo-Filho JD, et al. State-of-the-art in radiomics of hepatocellular carcinoma: a review of basic principles, applications, and limitations. *Abdom Radiol*. 2020;45(2):342–353.DOI:10.1007/s00261–019–02299–3.
16. Xu X, Zhang HL, Liu QP, et al. Radiomic analysis of contrast-enhanced CT predicts microvascular invasion and outcome in hepatocellular carcinoma. *J Hepatol*. 2019;70(6):1133–1144. doi:10.1016/j.jhep.2019.02.023
17. Ji GW, Zhu FP, Xu Q, et al. Radiomic features at contrast-enhanced CT predict recurrence in early stage hepatocellular carcinoma: a multi-institutional study. *Radiology*. 2020;294(3):568–579.DOI:10.1148/radiol.2020191470.
18. Lim KC, Chow PK, Allen JC, et al. Microvascular invasion is a better predictor of tumor recurrence and overall survival following surgical resection for hepatocellular carcinoma compared to the Milan criteria. *Ann Surg*. 2011;254(1):108–113. doi:10.1097/SLA.0b013e31821ad884
19. Hu HT, Wang Z, Huang XW, et al. Ultrasound-based radiomics score: a potential biomarker for the prediction of microvascular invasion in hepatocellular carcinoma. *Eur Radiol*. 2019;29(6):2890–2901. doi:10.1007/s00330-018-5797-0
20. Akai H, Yasaka K, Kunimatsu A, et al. Predicting prognosis of resected hepatocellular carcinoma by radiomics analysis with random survival forest. *Diagn Interv Imaging*. 2018;99(10):643–651. doi:10.1016/j.diii.2018.05.008
21. Cai W, He B, Hu M, et al. A radiomics-based nomogram for the preoperative prediction of posthepatectomy liver failure in patients with hepatocellular carcinoma. *Surg Oncol*. 2019;28:78–85. doi:10.1016/j.suronc.2018.11.013
22. Bodard S, Liu Y, Guinebert S, Kherabi Y, Asselah T. Performance of radiomics in microvascular invasion risk stratification and prognostic assessment in hepatocellular carcinoma: a meta-analysis. *Cancers*. 2023;15(3):743. doi:10.3390/cancers15030743
23. Feng L, Huang W, Pan X, et al. Predicting overall survival in hepatocellular carcinoma patients via a combined MRI radiomics and pathomics signature. *Transl Oncol*. 2025;51:102174. doi:10.1016/j.tranon.2024.102174
24. Zhou Y, He L, Huang Y, et al. CT-based radiomics signature: a potential biomarker for preoperative prediction of early recurrence in hepatocellular carcinoma. *Abdom Radiol*. 2017;42(6):1695. doi:10.1007/s00261-017-1072-0
25. Hinshaw DC, Shevde LA. The tumor microenvironment innately modulates cancer progression. *Cancer Res*. 2019;79(18):4557–4566. doi:10.1158/0008-5472.CAN-18-3962
26. Shi JY, Ma LJ, Zhang JW, et al. FOXP3 is a HCC suppressor gene and acts through regulating the TGF-β/Smad2/3 signaling pathway. *BMC Cancer*. 2017;17(1):648.DOI:10.1186/s12885–017–3633–6.
27. Michaeli J, Shaul ME, Mishalian I, et al. Tumor-associated neutrophils induce apoptosis of non-activated CD8 T-cells in a TNFα and NO-dependent mechanism, promoting a tumor-supportive environment. *Oncoimmunology*. 2017;6(11):e1356965. doi:10.1080/2162402X.2017.1356965
28. Dong P, Ma L, Liu L, et al. CD86+/CD206+, diametrically polarized tumorassociated macrophages, predict hepatocellular carcinoma patient prognosis. *Int J Mol Sci*. 2016;17(3):320. doi:10.3390/ijms17030320
29. Goltsev Y, Samusik N, Kennedy-Darling J, et al. Deep profiling of mouse splenic architecture with CODEX multiplexed imaging. *Cell*. 2018;174(4):968–981.e15. doi:10.1016/j.cell.2018.07.010
30. Schürch CM, Bhate SS, Barlow GL, et al. Coordinated cellular neighborhoods orchestrate antitumoral immunity at the colorectal cancer invasive. *Front Cell*. 2020;182(5):1341–1359. doi:10.1016/j.cell.2020.07.005

31. Phillips D, Schürch CM, Khodadoust MS, Kim YH, Nolan GP, Jiang S. Highly multiplexed phenotyping of immunoregulatory proteins in the tumor microenvironment by CODEX tissue imaging. *Front Immunol*. 2021;12:687673. doi:10.3389/fimmu.2021.687673
32. Phillips D, Matusiak M, Gutierrez BR, et al. Immune Cell Topography Predicts Response to PD-1 Blockade in Cutaneous T Cell Lymphoma. *medRxiv*. 2020. doi:10.1101/2020.12.06.20244913
33. Liu A, Liu B, Duan X, et al. Development of a novel combined nomogram model integrating rad-score, age and ECOG to predict the survival of patients with hepatocellular carcinoma treated by transcatheter arterial chemoembolization. *J Gastrointest Oncol*. 2022;13(4):1889–1897. doi:10.21037/jgo-22-548
34. Piñero F, Dirchwolf M, Pessôa MG. Biomarkers in Hepatocellular Carcinoma: diagnosis, Prognosis and Treatment Response Assessment. *Cells*. 2020;9(6):1370. doi:10.3390/cells9061370
35. Erstad DJ, Tanabe KK. Prognostic and therapeutic implications of microvascular invasion in hepatocellular carcinoma. *Ann Surg Oncol*. 2019;26(5):1474–1493. doi:10.1245/s10434-019-07227-9
36. Casadei-Gardini A, Orsi G, Caputo F, Ercolani G. Developments in predictive biomarkers for hepatocellular carcinoma therapy. *Expert Rev Anticancer Ther*. 2020;20(1):63–74. doi:10.1080/14737140.2020.1712198
37. Marrero JA, Kudo M, Bronowicki JP. The challenge of prognosis and staging for hepatocellular carcinoma. *Oncologist*. 2010;15(Suppl 4):23–33. doi:10.1634/theoncologist.2010-S4-23
38. Gillies RJ, Kinahan PE, Hricak H. Radiomics: images are more than pictures, they are data. *Radiology*. 2016;278(2):563–577. doi:10.1148/radiol.2015151169
39. Deng PZ, Zhao BG, Huang XH, et al. Preoperative contrast-enhanced computed tomography-based radiomics model for overall survival prediction in hepatocellular carcinoma. *World J Gastroenterol*. 2022;28(31):4376–4389. doi:10.3748/wjg.v28.i31.4376
40. Niu J, Li W, Liang C, et al. EGF promotes DKK1 transcription in hepatocellular carcinoma by enhancing the phosphorylation and acetylation of histone H3. *Sci Signal*. 2020;13(657):eabb5727. doi:10.1126/scisignal.abb5727
41. Chen L, Li M, Li Q, Wang CJ, Xie SQ. DKK1 promotes hepatocellular carcinoma cell migration and invasion through β-catenin/MMP7 signaling pathway. *Mol Cancer*. 2013;12(1):157. doi:10.1186/1476-4598-12-157
42. Yu B, Yang X, Xu Y, et al. Elevated expression of DKK1 is associated with cytoplasmic/nuclear β-catenin accumulation and poor prognosis in hepatocellular carcinomas. *J Hepatol*. 2009;50(5):948–957. doi:10.1016/j.jhep.2008.11.020
43. Jing M, Qiong L, Wang Z, Xiong X, Fu Y, Yan W. Histone H3 activates caspase-1 and promotes proliferation and metastasis in hepatocellular carcinoma. *Int J Med Sci*. 2023;20(5):689–701. doi:10.7150/ijms.76580
44. Pan W, Li W, Zhao J, et al. lncRNA-PDPK2P promotes hepatocellular carcinoma progression through the PDK1/AKT/caspase 3 pathway. *Mol Oncol*. 2019;13(10):2246–2258. doi:10.1002/1878-0261.12553
45. Liu X, He Y, Li F, et al. Caspase-3 promotes genetic instability and carcinogenesis. *Mol Cell*. 2015;58(2):284–296. doi:10.1016/j.molcel.2015.03.003
46. Zhang S, Xiao Q, Shi Z, et al. Caspase polymorphisms and prognosis of hepatocellular carcinoma. *PLoS One*. 2017;12(4):e0176802. doi:10.1371/journal.pone.0176802
47. Cho S, Lee JH, Cho SB, et al. Epigenetic methylation and expression of caspase 8 and survivin in hepatocellular carcinoma. *Pathol Int*. 2010;60:203–211. doi:10.1111/j.1440-1827.2009.02507.x
48. Deng B, Liu F, Luo L, Wei Y, Li B, Yang H. CASP3 genetic polymorphisms and risk of hepatocellular carcinoma: a case-control study in a Chinese population. *Tumour Biol*. 2016;37(7):8985–8991. doi:10.1007/s13277-015-4779-y